On the de Haas–van Alphen oscillations in quasi-two-dimensional metals: effect of the Fermi surface curvature

2007 J. Phys.: Condens. Matter 19 176227

(http://iopscience.iop.org/0953-8984/19/17/176227)

IOP PUBLISHING JOURNAL OF PHYSICS: CONDENSED MATTER

J. Phys.: Condens. Matter **19** (2007) 176227 (14pp) doi:10.1088/0953-8984/19/17/176227

On the de Haas–van Alphen oscillations in quasi-two-dimensional metals: effect of the Fermi surface curvature

Natalya A Zimbovskaya

Department of Physics and Electronics, University of Puerto Rico at Humacao, Humacao, PR 00791, USA

Received 4 November 2006, in final form 6 February 2007
Published 16 April 2007
Online at stacks.iop.org/JPhysCM/19/176227

Abstract

Here, we present the results of theoretical analysis of the de Haas–van Alphen oscillations in quasi-two-dimensional normal metals. We have studied the effects of the Fermi surface (FS) shape on these oscillations. It is shown that the effects could be revealed and well pronounced when the FS curvature becomes zero at cross-sections with extremal cross-sectional areas. In this case, both the shape and amplitude of the oscillations could be significantly changed. Also, we analyse the effect of the FS local geometry on the angular dependences of the oscillation amplitudes when the magnetic field is tilted away from the FS symmetry axis by the angle θ. We show that a peak appears at $\theta \approx 0^\circ$ whose height could be of the same order as the maximum at the Yamaji angle. This peak emerges when the FS includes zero-curvature cross-sections of extremal areas. Such a maximum was observed in experiments on α-$(BETS)_4TIHg(SeCN)_4$. The results that were obtained could be applied to organic metals and other quasi-two-dimensional compounds.

1. Introduction

Magnetic quantum oscillations are well known as a powerful tool used repeatedly in studies of the electronic properties of various conventional metals [1]. The theory of quantum oscillatory phenomena, such as de Haas–van Alphen oscillations in the magnetization and Shubnikov–de Haas oscillations in the magneto-resistivity of conventional three-dimensional metals, was derived by Lifshitz and Kosevich (LK) in their well-known work [2]. This theory was employed succesfully to extract valuable information concerning electron band-structure parameters from experimentally measured magnetic quantum oscillations.

In the last two decades quasi-two-dimensional (Q2D) materials with metallic-type conductivity (e.g. organic metals, intercalated compounds and some others) have attracted substantial interest, and extensive efforts have been applied to study their electronic characteristics. Magnetic quantum oscillations are frequently used as a tool in these

studies [3, 4]. A theory of magnetic oscillations in Q2D materials was proposed in several works (see e.g. [5–12]). Significant progress has already been made in developing the theory, but still there remain some significant points that have not been taken into account so far. The purpose of the present work is to contribute to the theory of de Haas–van Alphen oscillations in Q2D conductors by analysing one of these points, namely the effect of Fermi surface (FS) curvature on the amplitude and shape of the oscillations.

It has already been shown that local geometrical features of the FS may strongly affect quantum oscillations of elastic constants in both conventional and Q2D metals [13, 14], so one has grounds to expect similar manifestations in the magnetization oscillations. The effect of the FS local geometry on quantum oscillations in various observables could easily be given an explanation. In general, quantum oscillations are specified with contributions from the vicinities of effective cross-sections of the FS. These are cross-sections with minimum and maximum sectional areas. When the FS curvature becomes zero at an effective cross-section, the number of electrons associated with the latter increases, and their response is enhanced. This may significantly strengthen the oscillations originating from such cross-sections and change their shape and phase.

2. The model

The FSs of Q2D metals are known to be systems of weakly rippled cylinders. Accordingly, the current theory adopts the tight-binding approximation to describe the energy–momentum relation for the charge carriers. So, the energy spectrum could be written as follows:

$$E(\mathbf{p}) = \sum_{n=0} E_n(p_x, p_y) \cos\left(\frac{n p_z d}{\hbar}\right). \tag{1}$$

Here, the z axis is assumed to be perpendicular to the conducting layers; p_x, p_y, p_z are the quasi-momentum $\mathbf{p}$ coordinates, and d is the interlayer distance. The dependence of the energies E_n of p_x, p_y is introduced in equation (1) to take into account the anisotropies of the energy spectrum in the conducting layer planes. Due to the weakness of the interlayer interactions in Q2D conductors, the coefficient $E_0(p_x, p_y)$ is much greater than the remaining coefficients in the Fourier series in equation (1). Usually, in studies of magnetic quantum oscillations in Q2D conductors, the general energy–momentum relation (1) is simplified. The anisotropy of the energy spectrum in the layer planes is neglected, and only the first two perms in the sum over 'n' are kept. Then we arrive at the following simple model for a Q2D Fermi surface:

$$E(\mathbf{p}) = \frac{\mathbf{p}_\perp^2}{2m_\perp} - 2t\cos\left(\frac{p_z d}{\hbar}\right) \tag{2}$$

where $\mathbf{p}_\perp$ is the quasi-momentum projection on the layer plane, and $m_\perp$ is the effective mass corresponding to the motion of quasi-particles in this plane. The parameter t in this expression (2) is the interlayer transfer integral whose value determines how much the FS is warped. When t goes to zero, the FS becomes perfectly cylindrical.

Within this commonly used approximation, the FS profile is established completely. When a strong magnetic field $\mathbf{B}$ is applied along the normal to the layers ($\mathbf{B} = (0, 0, B)$), the FS Gaussian curvature at the effective cross-sections K_{ex} is given by:

$$K_{\mathrm{ex}} = -\frac{1}{2A_{\mathrm{ex}}}\left(\frac{\mathrm{d}^2 A}{\mathrm{d}p_z^2}\right) = \pm\frac{2\pi t m_\perp}{A_{\mathrm{ex}}}\left(\frac{d}{\hbar}\right)^2 \tag{3}$$

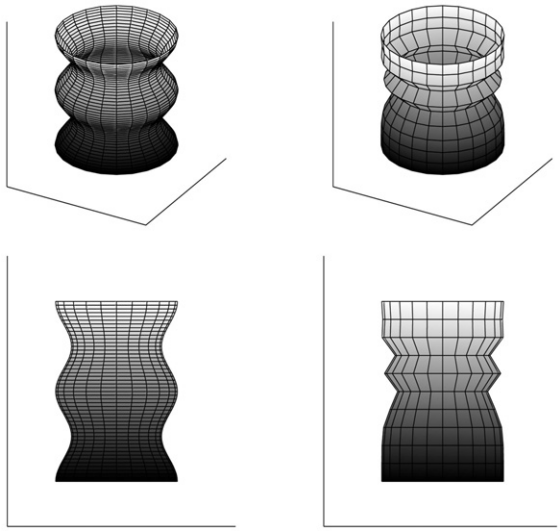

Figure 1. Schematic plots of a Fermi surface with a cosine warping corresponding to the model (2) (left), and a Fermi surface of a complex profile including cross-sections with maximum areas where the FS curvature becomes zero (right).

where $(\mathrm{d}^2A/\mathrm{d}p_z^2)_{\mathrm{ex}}$ means that the second derivative is calculated at the effective cross-section. and A_{ex} is the cross-sectional area. So, the curvature takes on values that are proportional to those of the interlayer transfer integral t, and it becomes zero only when the latter turns zero and the FS passes into a perfect unwarped cylinder.

However, there are grounds to believe that the FSs of some realistic Q2D conductors possess more complex geometries than those described by equation (2). For instance, in experiments on magnetic quantum oscillations in the layered perovskite oxide Sr_2RuO_4 [15, 16], it was shown that, to describe the FS of this material adequately, one must take into consideration at least four terms in the expansion (1). Here, we consider the Fermi cylinder corrugation of an arbitrary shape, provided that the cylinder remains a surface of revolution. Separating out the first term in the expansion (1), we may rewrite the energy–momentum relation in the form [17]:

$$E(\mathbf{p}) = \frac{\mathbf{p}_\perp^2}{2m_\perp} - 2t\epsilon\left(\frac{p_z d}{\hbar}\right) \tag{4}$$

where

$$\epsilon\left(\frac{p_z d}{\hbar}\right) = \sum_{n=1}^{\infty} \epsilon_n \cos\left(\frac{n p_z d}{\hbar}\right) \tag{5}$$

with $\epsilon_n = -E_n/2t$. It follows from this expression that $\epsilon(p_z d/\hbar)$ is an even periodic function of p_z whose period equals $2\pi\hbar/d$. Omitting all terms with $n > 1$ and assuming $E = 2t$, we may reduce our energy–momentum relation (4) to the simple form (2). By introducing this expression we obtain opportunities to describe Q2D FSs of various profiles (see figure 1) and to analyse the influence of their fine geometrical features on the de Haas–van Alphen oscillations. As shown below, these studies bring some non-trivial results which could not be obtained within the simple approximation (2).

3. Quantum oscillations in magnetization

We start from the standard expression for the longitudinal magnetization:

$$M_{\parallel}(B,T,\mu) \equiv M_z(B,T,\mu) = -\left(\frac{\partial\Omega}{\partial B}\right)_{T,\mu}. \tag{6}$$

Here, the magnetization depends on the temperature T and the chemical potential μ. The latter itself is a function of the magnetic field and temperature, and oscillates in strong magnetic fields. The expression for the thermodynamic potential can be written in the usual fashion:

$$\Omega(B,T,\mu) = -T\sum \ln\left\{1+\exp\left[\frac{\mu-E}{T}\right]\right\} \tag{7}$$

where the summation is carried over all possible states of quasi-particles. When a strong magnetic field is applied, the quasi-particles have the Landau energy spectrum, so the expression (4) takes the form:

$$E_{n,\sigma}(p_z) = \hbar\omega\left(n+\frac{1}{2}\right) + \sigma\frac{1}{2}g\hbar\omega_0 - 2t\epsilon\left(\frac{p_z d}{\hbar}\right). \tag{8}$$

Here, ω is the cyclotron frequency and $\omega_0 = \beta B$; β is the Bohr magneton, σ is the spin quantum number and g is the spin splitting coefficient (g-factor). Accordingly, we rewrite equation (7) as follows:

$$\Omega(B,T,\mu) = -\frac{T\omega}{(2\pi\hbar)^2}\sum_{n,\sigma}\int_{-\pi\hbar/d}^{\pi\hbar/d}\ln\left\{1+\exp\left[\frac{\mu-E_{n,\sigma}(p_z)}{T}\right]\right\}m_{\perp}\,\mathrm{d}p_z. \tag{9}$$

In further consideration, we assume as usual that the cyclotron quantum $\hbar\omega$ is small compared to the chemical potential μ. Then we employ the Poisson summation formula:

$$\sum_{n=0}^{\infty} f\left(n+\tfrac{1}{2}\right) = \int_0^{\infty} f(x)\left[1+2\,\mathrm{Re}\sum_{r=1}^{\infty}(-1)^r\exp(2\pi\mathrm{i}rx)\right]\mathrm{d}x. \tag{10}$$

Using this formula, the expression for the thermodynamic potential can be presented as a sum of a monotonic term Ω_0 and an oscillating correction $\Delta\Omega$:

$$\Delta\Omega = \frac{\mathrm{i}}{4\pi^2\hbar\lambda^2}\sum_{\sigma}\sum_{r=1}^{\infty}\frac{(-1)^r}{r}\int_0^{\infty}\frac{I(E_\sigma)\,\mathrm{d}E}{1+\exp[(E_\sigma-\mu)/T]}. \tag{11}$$

The function $I(E_\sigma)$ is given by:

$$I(E_\sigma) = 2\mathrm{i}\int\exp\left[\mathrm{i}r\frac{\lambda^2}{\hbar^2}A(E_\sigma,p_z)\right]\mathrm{d}p_z \tag{12}$$

where λ is the magnetic length and $A(E_\sigma, p_z)$ is the cross-sectional area.

Until this point we followed LK theory in the derivation of the expression for $\Delta\Omega$. As a result we arrived at equations (11) and (12), which are valid for conventional 3D metals as well as for Q2D and perfectly 2D conductors. Diversities in the expressions for $\Delta\Omega$ appear in the course of calculations of the function $I(E_\sigma)$. These calculations yield different results for different FS geometries. In deriving the standard LK formula it is assumed that the FS curvature is non-zero at the effective cross-sections with the extremal areas, and $I(E_\sigma, p_z)$ is approximated using the stationary phase method. For 2D metals the calculations of $I(E_\sigma)$ are trivial, for the FS is a cylinder and the cross-sectional area A does not depend on p_z. Obviously, in this case the FS curvature is zero everywhere. The oscillating part of the thermodynamic potential Ω for a 2D metal takes on the form:

$$\Delta\Omega = N\hbar\omega\left(\frac{B}{F}\right)\sum_{r=1}^{\infty}\frac{(-1)^r}{(\pi r)^2}R_T(r)R_S(r)\cos\left(\frac{2\pi rF}{B}\right). \tag{13}$$

Here, $F = cA/2\pi\hbar e$, N is the density of charge carriers, and $R_T(r)$ and $R_S(r)$ describe the effects of temperature and spin splitting, respectively. Also, the scattering of electrons deteriorates magnetic quantum oscillations, for it causes energy-level broadening. The simplest way to account for the effects of electron scattering on the oscillation amplitudes is to introduce an extra damping factor $R_D(r)$ (Dingle factor) into the expression (13). The usual approximation for the latter has the form $R_D(r) = \exp(-2\pi r/\omega\tau)$ [1], where τ is the scattering time of electrons. In further calculations we adopt this simple form for $R_D(r)$, for more sophisticated expressions are irrelevant to the main point of our subject. As a result we obtain:

$$\Delta\Omega = N\hbar\omega\left(\frac{B}{F}\right)\sum_{r=1}^{\infty}\frac{(-1)^r}{(\pi r)^2}R_T(r)R_S(r)R_D(r)\cos\left(\frac{2\pi r F}{B}\right)$$
$$\equiv N\hbar\omega\left(\frac{B}{F}\right)\sum_{r=1}^{\infty}\frac{(-1)^r}{(\pi r)^2}R(r)\cos\left(\frac{2\pi r F}{B}\right). \tag{14}$$

Correspondingly, we arrive at the following result for the oscillating part of the longitudinal magnetization [10]:

$$\Delta M_{\|} = -2N\beta\frac{\omega}{\omega_0}\sum_{r=1}^{\infty}\frac{(-1)^r}{\pi r}R(r)\sin\left(2\pi r\frac{F}{B}\right). \tag{15}$$

Taking into account the p_z-dependent term in the charge carriers' energy spectrum within the approximation (2), one can expand the integrand in equation (12) in Bessel functions and easily carry out integration over p_z. Then $\Delta M_{\|}$ takes the form [18]:

$$\Delta M_{\|} = -2N\beta\frac{\omega}{\omega_0}\sum_{r=1}^{\infty}\frac{(-1)^r}{\pi r}R(r)J_0\left(\frac{4\pi r t}{\hbar\omega}\right)\sin\left(2\pi r\frac{F}{B}\right). \tag{16}$$

When FS warping is negligible ($t \ll \hbar\omega$) this expression passes into the previous formula (15) describing the magnetization of a 2D metal. In the opposite limit ($t > \hbar\omega$) one can use the corresponding asymptotic for the Bessel functions. As a result the expression for $\Delta M_{\|}$ is transformed into a form similar to the LK result for conventional 3D metals:

$$\Delta M_{\|} = -2N\beta\frac{\omega}{\omega_0}\sqrt{\frac{\hbar\omega}{2\pi^2 t}}\sum_{r=1}^{\infty}\frac{(-1)^r R(r)}{\pi r^{3/2}}\sin\left(2\pi r\frac{F}{B}\right)\cos\left(\frac{4\pi r t}{\hbar\omega}-\frac{\pi}{4}\right)$$
$$= -N\beta\frac{\omega}{\omega_0}\sqrt{\frac{\hbar\omega}{2\pi^2 t}}\sum_{r=1}^{\infty}\frac{(-1)^r R(r)}{\pi r^{3/2}}$$
$$\times\left\{\sin\left(\frac{2\pi r F_{\max}}{B}-\frac{\pi}{4}\right)+\sin\left(\frac{2\pi r F_{\min}}{B}+\frac{\pi}{4}\right)\right\} \tag{17}$$

where $F_{\max} = FA_{\max}/A$, $F_{\min} = FA_{\min}/A$, and $A_{\max}$ and $A_{\min}$ are the maximum and minimum cross-sectional areas, respectively. As before, A is the cross-sectional area of the incorrugated cylindrical FS. Before we proceed, we remark again that the commonly used approximation (2) is not suitable for analysing the effects of the FS shape in Q2D metals. Within this model, the resulting formulae for ΔM are either reduced to the 2D limit (equation (15)) or they describe only cosine warped profiles of the FS without any variations (equations (16) and (17)). In both cases some important features of the oscillations could be missed.

We may expect the effect of FS curvature on the magnetization oscillations to appear when the FS warping is distinct ($t > \hbar\omega$). To analyse these effects we return back to our generalized energy–momentum relation (4). Then we assume that the FS curvature becomes zero at the effective cross-section at $p_z = p^*$. Then, as follows from the expression for the FS

curvature (3), $\mathrm{d}^2A/\mathrm{d}p_z^2$ equals zero at $p_z = p^*$, so we can write the following approximation for the cross-sectional area:

$$A(p_z) \approx A_{\mathrm{ex}} \pm \frac{1}{(2l)!}\left|\frac{\mathrm{d}^{2l}A}{\mathrm{d}p_z^{2l}}\right|_{p_z=p^*}(p_z - p^*)^{2l} \tag{18}$$

where $l > 1$.

Performing integration in parts in the expression (11), we obtain

$$\Delta\Omega = \frac{\hbar\omega}{\pi^2\hbar\lambda^2}\sum_{r=1}^{\infty}\frac{(-1)^2}{(\pi r)^2}R(r)\int_0^{\pi\hbar/d}\cos\left(\frac{r\lambda^2}{\hbar^2}A(p_z)\right)\mathrm{d}p_z. \tag{19}$$

Then, using the approximation (18) and applying the stationary phase method to compute the integral over p_z in expression (19), we obtain the following result for the contribution $\delta\Omega$ from the nearly cylindrical cross-section to the oscillating part of Ω:

$$\Delta\Omega = 2N\alpha_l\left(\frac{B}{2F}\right)^{\rho}\hbar\omega\sum_{r=1}^{\infty}\frac{(-1)^r}{(\pi r)^{\rho+1}}R(r)\cos\left(2\pi r\frac{F_{\mathrm{ex}}}{B}\pm\frac{\pi}{4l}\right). \tag{20}$$

Here, $\rho = 1 + 1/2l$;

$$\alpha_l = \frac{A_{\mathrm{ex}}}{V_0}\Gamma(\rho)\left(\frac{(2l)!A_{\mathrm{ex}}}{2\pi m_\perp t\left|\mathrm{d}^{2l}\epsilon/\mathrm{d}p_z^{2l}\right|_{p_z=p^*}}\right)^{1/2l} \tag{21}$$

where V_0 is the FS volume in a single Brillouin zone, and $\Gamma(\rho)$ is the gamma function. Based on this expression (20), we get the corresponding term in the oscillating part of the magnetization:

$$\begin{aligned}\Delta M_{\parallel} &= -2N\alpha_l\beta\left(\frac{B}{F}\right)^{1/2l}\frac{\omega}{\omega_0}\sum_{r=1}^{\infty}\frac{(-1)^r}{(\pi r)^{\rho}}R(r)\sin\left(2\pi r\frac{F_{\mathrm{ex}}}{B}\pm\frac{\pi}{4l}\right)\\ &\equiv -2N\xi_l\left(\frac{\hbar\omega}{t}\right)^{1/2l}\sum_{r=1}^{\infty}\frac{(-1)^r}{(\pi r)^{\rho}}R(r)\sin\left(2\pi r\frac{F_{\mathrm{ex}}}{B}\pm\frac{\pi}{4l}\right)\end{aligned} \tag{22}$$

where

$$\xi_l = \frac{A_{\mathrm{ex}}}{V_0}\Gamma(\rho)\left(\frac{(2l)!}{\left|\mathrm{d}^{2l}\epsilon/\mathrm{d}p_z^{2l}\right|_{p_z=p^*}}\right)^{1/2l}. \tag{23}$$

To arrive at the complete expression for $\Delta M_{\parallel}$ we must sum up terms originating from all effective cross-sections of the FS.

The FS shape near $p_z = p^*$ is determined by the shape parameter l. When $l = 1$ the FS has non-zero curvature at the cross-section considered. In this case, equation (22) agrees with the well-known LK result. Assuming that there are two extremal cross-sections (with the minimum and maximum cross-sectional areas, respectively) and summing up the contribution from both, we can easily transform our result (22) into the form (17).

When $l \gg 1$ we may roughly estimate $\left|\mathrm{d}^{2l}\epsilon/\mathrm{d}p_z^{2l}\right|_{p_z=p^*}$ as $(2l)^{2l+1}/(2l+1)$ and $(2l)!$ as $\exp[(2l+2)\ln(2l+2)]$ (see [19]). So, $\lim_{l\to\infty}\xi_l = 1/2$, and equation (22) passes into the expression (15) describing magnetization oscillations in 2D conductors multiplied by $1/2$. This extra factor appears because the expression (22) describes the contribution from a single nearly cylindrical cross-section of the FS. When the shape parameter for both effective cross-sections goes to infinity, their contributions to the magnetization oscillations become identical and, putting them together, we arrive at expression (15). In general, one may treat l as a phenomenological parameter whose actual value can be found from experiments. The greater is the value of this parameter, the closer is the FS to a cylinder near $p_z = p^*$.

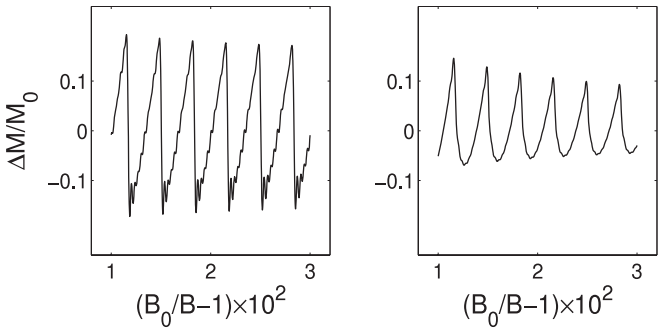

Figure 2. De Haas–van Alphen oscillations described by equation (22) for $l = 4$ (left panel) and $l = 1$ (right panel). Calculations are carried out for $T = T_D = 0.5$ K, $B_0 = 10$ T, and $F/B_0 = 300$; T_D is the Dingle temperature, and $M_0 = 2N\beta\omega/\omega_0$.

Oscillations in magnetization described by expression (22) vary in magnitude, shape and phase, depending on the value of the shape parameter l which determines the FS local geometry near the effective cross-section. This is illustrated in figure 2. As shown in this figure, when there is close proximity of the FS near $p_z = p^*$ to a cylinder, the oscillations are saw-toothed and resemble those occuring in 2D metals [7, 11] or originating from cylindrical segments of the FSs in conventional 3D metals [20, 21]. When the FS curvature takes on a non-zero value at $p_z = p^*$ ($l = 1$), the oscillations are similar to those in conventional metals. Here, we emphasize the difference between our result (22) and the expression (16). Using the latter, one could easily obtain saw-toothed oscillations typical for 2D metals, but only for small values of the transfer integral t ($t \ll \hbar\omega$) when FS crimping is negligible. The present result (22) shows that the oscillation shape and phase may be determined not by the value of t itself but rather by the form of the function $\epsilon(p_z d/\hbar)$ specifying the FS profile. The saw-toothed oscillations in magnetization could occur at $t \sim \hbar\omega$, when the FS curvature becomes zero at an effective cross-section. To ease the interpretation of this point, one may imagine an FS shaped as a step-like cylinder. The curvature of such an FS is zero everywhere, and oscillations from both kinds of the cross-sections (with minimum and maximum cross-sectional areas, respectively) should be similar to those in 2D metals. Nevertheless, the difference in the cross-sectional areas (the FS crimping) could be well pronounced, and a beat effect could be manifested. Obviously, this effect is absent when $t \ll \hbar\omega$ and the FS warping is negligible.

Also, it may happen that the FS curvature becomes zero at some effective cross-sections and remains non-zero at the rest of them. Then the contributions from zero-curvature cross-sections ($l > 1$) would exceed in magnitude those originating from the oridinary cross-sections ($l = 1$). This follows from expression (22), where the factor $(\hbar\omega/t)^{1/2l}$ ($\hbar\omega < 1$) is included. Depending on the value of the shape parameter l, this factor takes on values between $(\hbar\omega/t)^{1/2}$ ($l = 1$) and 1 ($l \to \infty$). So, when there is close proximity of the FS to a pure cylinder at some extremal cross-sections, the contributions from these cross-sections will predominate, and they will determine the shape and amplitude of the magnetization oscillations on the whole.

4. The effect of the chemical potential oscillations

It is known that the chemical potential μ oscillates in strong (quantizing) magnetic fields. These oscillations and the oscillations in the magnetization are closely related and described by similar series. The chemical potential is determined by the equation:

$$N = \left(\frac{\partial \Omega}{\partial \mu}\right)_{T,B}. \tag{24}$$

When the quantizing magnetic field is applied, the charge carrier density has an oscillating correction $\Delta N(\mu)$:

$$N = N_0(\mu) + \Delta N(\mu) \tag{25}$$

where N_0 is the charge carrier density at $B = 0$. Provided that the charge carrier density is fixed, this correction is to be balanced by an oscillating term, $\Delta\mu$, which appears in the chemical potencial due to the magnetic field. These corrections are related to each other by the equation [1]:

$$\Delta\mu \frac{\partial N_0}{\partial \mu} = \Delta N(\mu) \tag{26}$$

where $\partial N_0/\partial\mu \equiv D_0$ is the charge carrier density of states at the FS in the absence of the magnetic field. So, we have:

$$\Delta\mu(B) = \frac{1}{D_0}\left(\frac{\partial \Delta\Omega}{\partial \mu}\right)_{T,B}. \tag{27}$$

Assuming that the FS curvature becomes zero at the effective cross-section at $p_z = p^*$, using expression (20) for $\Delta\Omega$, and omitting smaller contributions from the remaining cross-sections of non-zero curvature, we obtain:

$$\Delta\mu = -\zeta_l \hbar\omega \sum_{r=1}^{\infty} \frac{(-1)^r}{(\pi r)^\rho} R(r) \sin\left(2\pi r \frac{F_{\rm ex}}{B} \pm \frac{\pi}{4l}\right). \tag{28}$$

Here, $\zeta_l = 4N\alpha_l(B/F)^\rho/\hbar\omega D_0$, and D_0 is the electron density of states at the FS in the absence of the magnetic field. The dimensionless factor ζ_l takes on small values of the order of $(\hbar\omega/E_{\rm F})^{1/2l}$. This result (28) as well as the expression for the oscillating part of magnetization (22) do not contradict the corresponding results for 2D and 3D metals reported in earlier works [10, 22]. For a conventional 3D metal whose FS has non-zero curvature at the effective cross-sections, the oscillating correction $\Delta\mu$ is very small compared to $E_{\rm F}$ ($\Delta\mu/E_{\rm F} \sim (\hbar\omega/E_{\rm F})^{3/2}$). Therefore it does not cause noticeable changes in de Haas–van Alphen oscillations. However, in the case of Q2D metals this correction could be more important [10, 11]. To analyse the effect of quantum oscillations in the chemical potential, one must take into account that the extremal cross-sectional areas, $A_{\rm ex}$, include corrections proportional to $\Delta\mu$, namely:

$$A_{\rm ex} = A_{\rm ex}(0) + 2\pi m_\perp \Delta\mu(B) \tag{29}$$

where $A_{\rm ex}(0)$ is the cross-sectional area in the absence of the magnetic field. Correspondingly, the argument of the cosine function in equation (20) must be written in the form:

$$2\pi r \frac{F_{\rm ex}}{B} \pm \frac{\pi}{4l} = 2\pi r\left(\frac{F_0^{\rm ex}}{B} + \frac{\Delta\mu}{\hbar\omega}\right) \pm \frac{\pi}{4l}. \tag{30}$$

To simplify further analysis, we keep only the first term in the expansion (28). Then we can employ the identity:

$$\exp\left[{\rm i}r\zeta_l R(1)\sin\left(2\pi\frac{F_0^{\rm ex}}{B} \pm \frac{\pi}{4l}\right)\right] = \sum_{n=-\infty}^{\infty} J_n\big(r\zeta_l R(1)\big)\exp\left[{\rm i}n\left(\frac{2\pi F_0^{\rm ex}}{B} \pm \frac{\pi}{4l}\right)\right] \tag{31}$$

where $J_n(r\zeta_l R(1))$ are the Bessel functions.

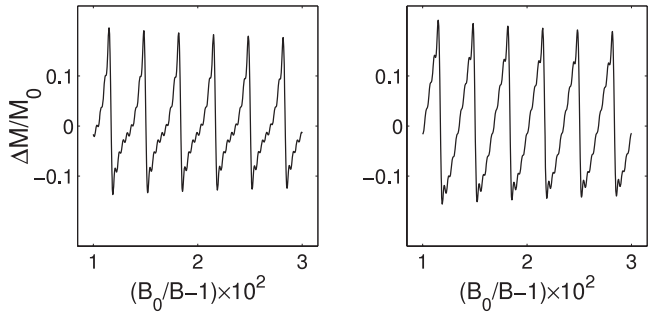

Figure 3. The effect of the chemical potential oscillations on the magnetization oscillations. The curves are plotted by taking into account the chemical potential oscillations according to equation (32) (left) and neglecting the latter (right). For both curves, $l = 4$ ($\rho = 1.125$) and the remaining parameters coincide with those used in plotting figure 2.

Using this identity we can write the expression for $\Delta M_{\|}$ as follows:

$$\Delta M_{\|} = -2N\alpha_l\beta\left(\frac{B}{F}\right)^{1/2l}\frac{\omega}{\omega_0}\sum_{s=1}^{\infty}\left\{A_s\sin\left(2\pi s\frac{F_0^{\rm ex}}{B}\pm\frac{\pi s}{4l}\right)\mp B_s\cos\left(2\pi s\frac{F_0^{\rm ex}}{B}\pm\frac{\pi s}{4l}\right)\right\}. \tag{32}$$

Here, the coefficients A_s, B_s are given by:

$$A_s = \sum_{r=1}^{\infty}\frac{(-1)^r R(r)}{(\pi r)^{\rho}}\left\{J_{r+s}\big(r\zeta_l R(1)\big)\cos\left(\frac{\pi(r+1)}{4l}\right) - J_{r-s}\big(r\zeta_l R(1)\big)\cos\left(\frac{\pi(r-1)}{4l}\right)\right\}; \tag{33}$$

$$B_s = \sum_{r=1}^{\infty}\frac{(-1)^r R(r)}{(\pi r)^{\rho}}\left\{J_{r+s}\big(r\zeta_l R(1)\big)\sin\left(\frac{\pi(r+1)}{4l}\right) - J_{r-s}\big(r\zeta_l R(1)\big)\sin\left(\frac{\pi(r-1)}{4l}\right)\right\}. \tag{34}$$

These formulae (32)–(34) are generalizations of the results obtained for 2D metals [11, 23, 24].

As follows from equations (32)–(34), the oscillating correction to the chemical potential may cause some changes in the amplitude and shape of the de Haas–van Alphen oscillations in Q2D metals. Keeping in mind that the damping factor $R(r)$ takes on values less than unity and reduces while r increases, we can write explicit expressions for the first few harmonics in the form:

$$\delta M_1 = 2N\alpha_l R(1)\pi^{-\rho}\sin\left(2\pi\frac{F_0^{\rm ex}}{B}\pm\frac{\pi}{4l}\right); \tag{35}$$

$$\delta M_2 = -2N\alpha_l R(2)(2\pi)^{-\rho}\left\{\sin\left(4\pi\frac{F_0^{\rm ex}}{B}\pm\frac{\pi}{4l}\right)+\frac{R^2(1)}{R(2)}2^{1/2l}\zeta_l\sin\left(4\pi\frac{F_0^{\rm ex}}{B}\pm\frac{\pi}{2l}\right)\right\}; \tag{36}$$

$$\delta M_3 = 2N\alpha_l R(3)(3\pi)^{-\rho}\left\{\sin\left(6\pi\frac{F_0^{\rm ex}}{B}\pm\frac{\pi}{4l}\right)+\frac{R(2)R(1)}{R(3)}\left(\frac{3}{2}\right)^{\rho}\zeta_l\sin\left(6\pi\frac{F_0^{\rm ex}}{B}\pm\frac{\pi}{2l}\right)\right\}. \tag{37}$$

So we see that the chemical potential oscillations do not affect the fundamental harmonic but they contribute to higher harmonics, causing changes to their amplitude and phase. Similar conclusions were recently drawn by analysing the effect of chemical potential oscillations on magnetization in 2D metals [11]. The effect depends on the FS local geometry. When the shape parameter l takes on greater values, the effect becomes stronger. As shown in figure 3,

for pronounced proximity of the FS to a cylinder near the effective cross-section ($l = 4$), a noticeable difference in the magnetization oscillation's shape and magnitude arises due to the effect of the chemical potential oscillations.

The correction from $\Delta\mu$ causes changes in the position of spin-splitting zeros in the harmonics of the de Haas–van Alphen oscillations. These changes have been studied before within the simple approximation (2) for the energy spectrum [25, 26]. It was shown that the spin-zero positions for the second and third harmonics are not completely determined with zeros in corresponding spin-splitting factors $R_S(2)$ and $R_S(3)$. They also depend on the values of $R(1)$ and $R(3)$ (which are dependent on temperature and scattering) and on the magnetic field. Here, we show that the spin-zero positions also depend on the FS geometry at the extremal cross-sections. This follows from the expressions (36) and (37).

5. Angular dependence of the oscillations amplitudes

The effect of FS curvature on quantum oscillations in the magnetization is expected to be very sensitive to the geometry of the experiments. The reason is that the effective FS cross-sections (with the minimum/maximum cross-sectional areas) run along the lines of zero curvature (if any) only in certain directions of the magnetic field. When the magnetic field is tilted away from such directions by the angle θ, the extremal cros-section slips from the nearly cylindrical strip on the FS containing a zero-curvature line. This results in a decrease in the oscillation's amplitude. The phase of the oscillations also changes. These angular dependences of the oscillations' amplitudes and phases differ radically in origin from the effect first described by Yamaji [27].

The Yamaji effect occurs due to the coincidence of the FS extremal areas $A_{\max}$ and $A_{\min}$ at certain angles of inclination of the magnetic field with respect to the FS symmetry axis. At such angles all the cross-sections on the FS have the same area, so the amplitude of the de Haas–van Alphen oscillations increases. The Yamaji effect originates from the periodicity of the p_z-dependent contribution to the charge carriers' energy spectrum, and it is unrelated to the presence/absence of zero-curvature lines on the relevant FS. Also, there is a crucial difference in the manifestations of the two effects. The angular dependence originating from the effects of the FS curvature reveals itself at very small values of θ, whereas the first maximum due to the Yamaji effect usually appears at $\theta \sim 10^\circ$ or even greater. To clarify the difference between the two effects further, we analyse the angular dependence of de Haas–van Alphen oscillation amplitudes, assuming that the FS curvature becomes zero at an extremal cross-section when the magnetic field is directed along the FS axis of symmetry.

We suppose that the magnetic field is inclined from the FS symmetry axis by the angle θ within the xz plane, and we employ the coordinate system whose z' axis is directed along the magnetic field. We use the energy–momentum relation given by equations (4) and (5), and we rewrite them in terms of new coordinates p'_z, p_y, p'_z ($p'_x = p_x\cos\theta + p_z\sin\theta$; $p'_z = p_z\cos\theta - p_x\sin\theta$). Changing variables in equations (4) and (5) and keeping in mind that $\sin\theta$ takes on very small values at small angles θ, we may present the energy–momentum relation for a weakly corrugated Fermi cylinder ($t \ll \mu$) in the form:

$$p_0^2 = p_x'^2\cos^2\theta + p_y^2 - 4m_\perp t\sum_{n=1}^{\infty}\epsilon_n\cos\left(\frac{nd}{\hbar}[p'_z\cos\theta + p'_x\sin\theta]\right) \tag{38}$$

where p_0 is the radius of the unwarped Fermi cylinder ($p_0 = \sqrt{A/\pi}$). Introducing polar coordinates in the cutting plane ($p'_x = p\cos\varphi$; $p_y = p\sin\varphi$), we may calculate the FS cross-sectional area provided that the magnetic field is tilted away from the FS symmetry

axis:

$$A(p_z', \theta) = \int_0^{2\pi} \mathrm{d}\varphi \int_0^{p} p\,\mathrm{d}p = A_0(\theta) + \Delta A(p_z', \theta). \tag{39}$$

Here,

$$A_0(\theta) = 2p_0^2 \int_0^{\pi/2} \frac{\mathrm{d}\varphi}{\cos^2\theta\cos^2\varphi + \sin^2\varphi} = \frac{A}{\cos\theta} \tag{40}$$

and

$$\Delta A(p_z', \cos\theta) = 2m_\perp t \sum_{n=1}^{\infty} \epsilon_n \int_0^{2\pi} \cos\left(\frac{np_z' d}{\hbar}\cos\theta + \frac{np_0 d}{\hbar}\tan\theta\cos\varphi\right)\mathrm{d}\varphi. \tag{41}$$

Then we can present the oscillating part of the longitudinal magnetization in the form:

$$\Delta M_\parallel = -2N\beta\frac{\omega}{\omega_0}\sum_{r=1}^{\infty}\frac{(-1)^r}{\pi r}\sin\left(\frac{2\pi r F(\theta)}{B} + \Phi_r(\theta)\right) Y_r(\theta). \tag{42}$$

Here, $Y_r(\theta) = \sqrt{C_r^2(\theta) + S_r^2(\theta)}$, $\Phi = \arctan[S_r(\theta)/C_r(\theta)]$, $F(\theta) = F/\cos\theta$,

$$C_r(\theta) = \frac{d}{2\pi\hbar\cos\theta}\int_{(-\pi\hbar/d)\cos\theta}^{(\pi\hbar/d)\cos\theta}\cos\left(\frac{r\lambda^2}{\hbar^2}\Delta A(p_z', \theta)\right)\mathrm{d}p_z', \tag{43}$$

$$S_r(\theta) = \frac{d}{2\pi\hbar\cos\theta}\int_{(-\pi\hbar/d)\cos\theta}^{(\pi\hbar/d)\cos\theta}\sin\left(\frac{r\lambda^2}{\hbar^2}\Delta A(p_z', \theta)\right)\mathrm{d}p_z'. \tag{44}$$

Expanding the integrand in (41) in Bessel functions, we can easily carry out the integration over φ. Then we get:

$$\Delta A(p_z', \cos\theta) = 4\pi m_\perp t\sum_{n=1}^{\infty}\epsilon_n\cos\left(\frac{np_z'}{\hbar}\cos\theta\right)J_0\left(\frac{np_0 d}{\hbar}\tan\theta\right). \tag{45}$$

The first term in this expansion coincides with the result given in the Yamaji work. The latter was obtained assuming simple cosine warping of the FS described by equation (2).

To analyse the effect of the FS curvature we assume that the curvature becomes zero at $p_z = \pi\hbar/d$. Requiring that $(\mathrm{d}^2A/\mathrm{d}p_z^2)_{p_z=\pi\hbar/d} = 0$ (see equation (3)) and keeping only the first two terms in the expansion (5), we obtain:

$$\epsilon\left(\frac{p_z d}{\hbar}\right) = \cos\left(\frac{p_z d}{\hbar}\right) + \frac{1}{4}\cos\left(\frac{2p_z d}{\hbar}\right). \tag{46}$$

In this case the cross-sectional area $A(p_z)$ near $p_z = \pi\hbar/d$ is approximated as:

$$A(p_z) = A(p_0) + \frac{\pi m_\perp t}{2}\left(\frac{d}{\hbar}\right)^4\left(p_z - \frac{\pi\hbar}{d}\right)^4. \tag{47}$$

Comparing this expression with equation (18), we conclude that the shape parameter $l = 2$.

Correspondingly, we must put $\epsilon_1 = 1$, $\epsilon_2 = 1/4$, $\epsilon_n = 0$ $(n > 2)$ into the general expression (46) for $\Delta A(p_z', \theta)$. As a result we get:

$$\Delta A(p_z', \cos\theta) = 4\pi m_\perp t\left[\cos\left(\frac{p_z' d}{\hbar}\cos\theta\right)J_0\left(\frac{p_0 d}{\hbar}\tan\theta\right) + \frac{1}{4}\cos\left(\frac{2p_z' d}{\hbar}\cos\theta\right)J_0\left(\frac{2p_0 d}{\hbar}\tan\theta\right)\right]. \tag{48}$$

To describe FSs possessing closer proximity to a perfect cylinder near a certain extremal cross-section, we must keep more terms in the expansion (5). For instance, assuming $\epsilon_1 = 1$,

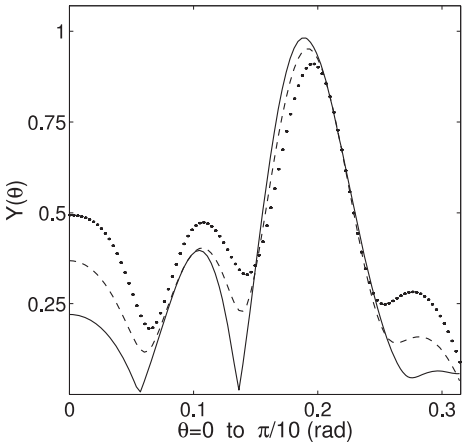

Figure 4. Angular dependences of the magnetization oscillation amplitudes. The curves are plotted assuming that $t/\hbar\omega = 0.5$ and $p_0 d/\hbar = 4\pi$. The shape parameter l takes on the values $l = 1$ (solid line), $l = 2$ (dashed line), and $l = 3$ (dotted line). The plotted curves are described by equations (42)–(44) ($r = 1$).

$\epsilon_2 = 2/5$, $\epsilon_3 = 1/15$, and $\epsilon_n = 0$ ($n > 3$), we ensure that both $\mathrm{d}^2A/\mathrm{d}p_z^2$ and $\mathrm{d}^4A/\mathrm{d}p_z^4$ become zero at $p_z = \pi\hbar/d$, which corresponds to $l = 3$. Similarly, at $\epsilon_1 = 1$, $\epsilon_2 = 1/2$, $\epsilon_3 = 1/7$, $\epsilon_4 = 1/56$, and $\epsilon_n = 0$ ($n > 4$), we obtain $l = 4$, and so forth. Substituting these numbers into the general expression (45) for $\Delta A(p_z', \cos\theta)$, and using the results to compute the functions $C_r(\theta)$ and $S_r(\theta)$ given by equations (43) and (44), we may finally calculate the factors $Y_r(\theta)$. The latter describe the desired angular dependence of the oscillations amplitudes.

Here, we carried out the calculations accepting $t/\hbar\omega = 0.5$ and $p_0 d/\hbar = 4\pi$ and keeping only the first term in the sum over r in equation (42). The resulting curves are presented in figure 4. The solid line in this figure is associated with the energy spectrum of the form (2). The corresponding FS has cosine warping and possesses non-zero curvature at the expremal cross-sections. The high peak at $\theta = 0.185$ (10.6°) corresponds to the first Yamaji maximum. The position of this peak is in agreement with the equation $(p_0 d/\hbar)\tan\theta = 3\pi/4$ (see [27]). Two preceding zeros originate from the beats. The remaining curves represent FSs whose curvature becomes zero at their minimum cross-sections at $\theta = 0$. We see that the closer the FS shape to that of a perfect cylinder in the vicinities of these cross-sections (the greater is the value of l), the greater is the amplitude of the oscillations near $\theta = 0$ and the smaller is the Yamaji maximum. At $l = 3$ the Yamaji maximum is approximately two times higher than the maximum at $\theta = 0$, whereas at $l = 1$ the ratio of the heights takes on a value close to 4. We may expect that at very close proximity of the FS to a cylinder near the extremal cross-section ($l \sim 10$), the amplitude maximum at $\theta = 0$ will exceed the Yamaji peak. Also, we see that the amplitudes of the oscillations associated with the FSs containing zero-curvature extremal cross-sections do not become zero at small angles θ. This is due to the fact that the FSs that are considered are warped cylinders whose curvature is zero at the cross-sections with minimum areas (such as $p_z = \pi\hbar/d$) but remains non-zero at the cross-sections with maximum areas (such as $p_z = 0$). The difference in the amplitudes of the oscillations originating from the FS local geometry near its extremal cross-sections prevents beats from being well manifested.

The angular dependence of the magnetization oscillation's amplitude resembling that presented in figure 4 was reported to be observed in experiments on the Q2D organic metal α-$(BETS)_2TIHg(SeCN)_4$ [28]. In these experiments a high peak in the amplitude was observed

when the magnetic field was directed along the axis of the corrugated cylinder which is part of the FS. When the field was tilted away from this axis by the angle θ, the amplitude decreased rapidly and reached approximately half of the initial value at $\theta \sim 5°$. A further increase in the angle θ caused small variations in the amplitude until another peak was reached at $\theta \sim 18°$. Identifying this second peak with the first Yamaji maximum, we may conjecture that the higher peak at $\theta = 0$ arises due to the presence of FS extremal cross-sections of zero curvature. The relation between the heights of the peaks reported in [27] gives grounds to expect that the nearly cylindrical segments of the α-$(BETS)_2TIHg(SeCN)_4$ Fermi surface (where the FS curvature becomes zero) are very close to perfect cylinders, so that the shape parameter l takes on values significantly greater than unity.

6. Conclusion

In summary, the present work aims to study the effect of the FS shape on the de Haas–van Alphen oscillations in Q2D conductors. Such analysis is important, for there exists a great deal of interest in studies of band-structure parameters and other electronic properties of these materials. Usually, a simple model for the electron spectrum (2) is employed to extract the relevant information from the experiments. This approximation has its limitations, so some problems arise in interpreting the experimental data (see, e.g., [15, 16, 28]). An important limitation of the current theory is that the latter misses the effects of the FS geometry assuming a simple cosine warping of the FS. Here, we lift this restriction on the FS shape. We show that the FS profile may significantly affect the quantum oscillations in magnetization if the FS curvature becomes zero at a cross-sectional area. Also, we show that the main characteristics of the oscillations are determined by two different factors, namely by the FS curvature at the effective cross-sections and the transfer integral, whereas the existing theory takes into account only the latter. These two factors work simultaneously, and their effects can be separated. As discussed above, features that are typical for 2D conductors can be revealed when the FS is rippled, provided that its curvature becomes zero at cross-sections with extremal areas.

The presence of zero-curvature effective cross-sections noticeably affects the angular dependences of the oscillation amplitudes. A maximum originating due to the FS local geometry can emerge. The height of this peak can be comparable to the height of the well-known Yamaji maximum and even exceed the latter. This agrees with the experimental results observed on the Q2D α-$(BETS)_2TIHg(SeCH)_4$ organic metal [28]. The proposed approach could be useful in analysing experiments on magnetization oscillations in Q2D conductors, especially those where saw-tooth features in the oscillations are well pronounced. It could help to extract important extra information concerning fine geometrical features of the FSs of such materials.

Acknowledgments

The author thanks G M Zimbovsky for help with the manuscript. This work was supported by the US National Science Foundation (NSF) Advance program SBE-0123654 and Puerto Rico Space Grant NGTS/40091.

References

[1] Shoenberg D 1984 *Magnetic Oscillations in Metals* (New York: Cambridge University Press)
Also, see, Zimbovskaya N A 2001 *Local Geometry of Fermi Surface and High-Frequency Phenomena in Metals* (New York: Springer)

[2] Lifshitz I M and Kosevich A M 1955 *Zh. Eksp. Teor. Fiz.* **29** 730
Lifshitz I M and Kosevich A M 1956 *Sov. Phys.—JETP* **2** 636 (Engl. Transl.)
[3] Wosnitza J 1996 *Fermi Surface of Low-Dimensional Organic Metals and Superconductors* (Berlin: Springer)
[4] Singleton J 2000 *Rep. Prog. Phys.* **63** 1111
[5] Vagner I D, Maniv T and Ehrenfreund E 1983 *Phys. Rev. Lett.* **51** 1700
[6] Jauregui K, Marchenko V I and Vagner I D 1990 *Phys. Rev.* B **41** 12922
[7] Harrison N, Bogaerts R, Reinders P H P, Singleton J, Blundell S J and Herlach F 1996 *Phys. Rev.* B **54** 9977
[8] Champel T 2001 *Phys. Rev.* B **64** 054407
[9] Grigoriev P D 2003 *Phys. Rev.* B **67** 144401
[10] Gvozdikov V M, Jansen A G M, Pesin D A, Vagner I D and Wyder P 2003 *Phys. Rev.* B **68** 155107
[11] Gvozdikov V M, Jansen A G M, Pesin D A and Vagner I D 2004 *Phys. Rev.* B **70** 245114
[12] Carrington A, Fletcher J D and Harima T 2005 *Phys. Rev.* B **71** 174505
[13] Zimbovskaya N A 2005 *Phys. Rev.* B **71** 024109
[14] Zimbovskaya N A and Birman J L 2002 *Int. J. Mod. Phys.* B **16** 1767
[15] Bergemann C, Julian S R, Mackenzie A P, Nishizaki S and Maeno Y 2000 *Phys. Rev. Lett.* **84** 2662
[16] Bergemann C, Mackenzie A P, Julian S R, Forsythe D and Ohmichi E 2003 *Adv. Phys.* **52** 639
[17] Zimbovskaya N A 1998 *Zh. Eksp. Teor. Fiz.* **113** 2229
Zimbovskaya N A 1998 *JETP* **86** 1220 (Engl. Transl.)
[18] Grigoriev P 2001 *Zh. Eksp. Teor. Fiz.* **119** 1257
Grigoriev P 2001 *JETP* **92** 1090 (Engl. Transl.)
[19] Gradstein I S and Ryzhik I M 1965 *Table of Integrals, Series and Products* (New York: Academic)
[20] Lacueva G and Overhauser A W 1992 *Phys. Rev. Lett.* **46** 1273
[21] Blanter Ya M, Kaganov M I and Posvyanskii D B 1995 *Phys—Usp.* **165** 178
[22] Gvozdikov V M 1984 *Sov. Phys.—Solid State* **26** 1560
[23] Wosnitza J, Wanka S, Hagel J, Balthes E, Harrison N, Schlueter J A, Kini A M, Geiser U, Montasham J, Winter R W and Gard G L 2000 *Phys. Rev.* B **61** 7383
[24] Wosnitza J, Gvozdikov V M, Hagel J, Meeson P J, Schlueter J A, Winter R W and Gard G L 2004 *Preprint* cond-mat/0412202
[25] Wosnitza J, Wanka S, Hagel J, Lohneysen H v, Qualls J S, Brooks J S, Balthes E, Schlueter J A, Geiser U, Mohtasham J, Winter R W and Gard G L 2001 *Phys. Rev. Lett.* **86** 508
[26] Nakano M 2000 *Phys. Rev.* B **62** 45
[27] Yamaji K 1989 *J. Phys. Soc. Japan* **58** 1520
[28] Pesotskii S I, Lyubovskii R B, Nizhankovskii V I, Biberacher W, Kartsovnic M V, Andres K, Perenboom A A, Kushch N D, Yagubskii E B and Kobayashi H 2000 *Zh. Eksp. Teor. Fiz.* **117** 604
Pesotskii S I, Lyubovskii R B, Nizhankovskii V I, Biberacher W, Kartsovnic M V, Andres K, Perenboom A A, Kushch N D, Yagubskii E B and Kobayashi H 2000 *JETP* **90** 527 (Engl. Transl.)